inorganics

MDPI

Article

Green Synthesis of Silver Nanoparticles Using *Artemisia vulgaris* Extract and Its Application toward Catalytic and Metal-Sensing Activity

Achyut Adhikari [1,*], Laxman Lamichhane [1], Anup Adhikari [1], Gobinda Gyawali [2], Debendra Acharya [3], Ek Raj Baral [4] and Kisan Chhetri [3,*]

[1] Central Department of Chemistry, Tribhuvan University, Kathmandu 44618, Nepal
[2] Department of Fusion Science and Technology, Sun Moon University, Asan 31460, Korea
[3] Department of Nano Convergence Engineering, Jeonbuk National University, Jeonju 561756, Korea
[4] Department of Chemistry, Research Institute of Physics and Chemistry, Jeonbuk National University, Jeonju 561756, Korea
* Correspondence: achyutraj05@gmail.com (A.A.); chhetrikisan88@jbnu.ac.kr (K.C.)

Abstract: Nonessential heavy metals are toxic to human health. In this study, mercury, a hazardous metal, was detected by colorimetric analysis using *Artemisia vulgaris*-mediated silver nanoparticles (AgNP) without any modification in an aqueous solution. The UV–vis spectroscopy showed a characteristic SPR band of Ag^0 at 418 nm, indicating the formation of AgNPs. The AgNPs were crystalline, with an average size of 7 nm, as calculated from the XRD data. The SEM images revealed the spherical and polycrystalline AgNPs within the agglomerated form. The FTIR spectra elucidated the functional group of the extract attached with the Ag^0. The broad, strong peak at 3632 cm^{-1} indicated the involvement of the -OH group of compounds of extract in reducing silver ions. The peak of EDX spectra around 3 keV confirmed the silver in the nanostructure. A colorimetric method was employed for the heavy metal sensing in the aqueous medium without modification of AgNPs suspension. The obtained AgNPs were found to be selective and highly sensitive toward Hg^{2+} ions. The AgNPs suspension turned colorless after adding 380 µL of 1 mM Hg^{2+}. The synthesized AgNPs showed the catalytic activity on reduction of 4-nitrophenol in the presence of $NaBH_4$ within 8 min with a rate constant of 1.21×10^{-2} s^{-1}. The outcome of these findings suggests that the application of *Artemisia vulgaris* influenced AgNPs for metal sensing and green catalysis.

Keywords: nanoparticle; silver nanoparticle; mercury sensor; green synthesis; catalysis

Citation: Adhikari, A.; Lamichhane, L.; Adhikari, A.; Gyawali, G.; Acharya, D.; Baral, E.R.; Chhetri, K. Green Synthesis of Silver Nanoparticles Using *Artemisia vulgaris* Extract and Its Application toward Catalytic and Metal-Sensing Activity. *Inorganics* **2022**, *10*, 113. https://doi.org/10.3390/inorganics10080113

Academic Editor: Huihui Li

Received: 5 July 2022
Accepted: 29 July 2022
Published: 4 August 2022

1. Introduction

Nanoparticles (NPs) exhibit enhanced or significantly improved properties based on specific characteristics, such as morphology, size, and distribution. Bulk and atomic structures differ in their properties, and metal NPs bridge the gap between them with their unique physicochemical properties, i.e., large surface area, high reactivity, large surface-to-volume ratio, spatial confinement, tunable pore size, and particle morphology. The NPs developed with noble metals, particularly Au, Ag, Pt, and Pd, are researched effectively [1]. Due to their unique physical and chemical properties, such as high thermal and electrical conductivity, good chemical stability, and nonlinear optical properties, silver nanoparticles (AgNPs) have piqued the interest of researchers over NPs made from other noble metals [2]. The shape, size, and composition of AgNPs can severely influence their efficacy; extensive research has been conducted to synthesize and characterize AgNPs.

Green and quick NP synthesis methods derived from plant extracts have gained popularity due to their convenience of use, underlying safety, and convenience [3]. Biological techniques employ the green chemistry criterion to replace harsh chemicals with natural products such as enzymes, phytochemicals, and biodegradable polymerase [4].

Biomolecules contained in plant parts, such as alkaloids, flavonoids, and various phenolic compounds (lignin, phenolic acids, tannins, and stilbenes), are responsible for the rapid reduction along with stabilizing and capping of metal salts [5]. These biomolecules affect the morphology of synthesized NPs [6,7]. It also determines the reduction potential of ions, which in turn determines the amount of NPs accumulated [8]. The exact mechanism based on AgNPs production by plants is not thoroughly studied. It is believed that biomolecules are responsible for the reduction of ions and the formation of AgNPs [9]. The green synthesis of metal NPs, reduction, capping, and stabilization steps occur, and the biomolecules, such as enzymes, proteins, sugars, etc., are present in the plant extract [10]. The principle involved in each plant may differ depending on the types of phytoconstituents, but the primary mechanism is ion reduction.

Heavy metals are referred to as heavy metals that adversely affect the environment and living organisms and possess a specific density of more than 5 g cm^{-3} [11]. Nonessential heavy metals, such as lead (Pb), chromium (Cr), cadmium (Cd), mercury (Hg), arsenic (As), and antimony (Sb), are non-biodegradable, highly toxic, and carcinogenic even at a trace level. Heavy metals enter the surroundings through human activities and natural means [12]. Heavy metals are up-taken from contaminated soil by plants and eventually passed along the food chain to herbivorous animals. Contamination of crops such as vegetables and cereals is a severe problem concerning contamination of humans. Consumption of toxic-heavy-metal-contaminated cereals and meat may risk human health [13]. When heavy metal enters our body, it combines with enzymes and proteins to form strongly stable chemical bonds and thus inhibits regular functioning. The equations below show their reactions during the formation of bonds with the sulfhydryl groups (-SH) of cysteine and sulfur atoms of methionine (-SCH_3) (Scheme 1) (Duruibe et al., 2007) [14].

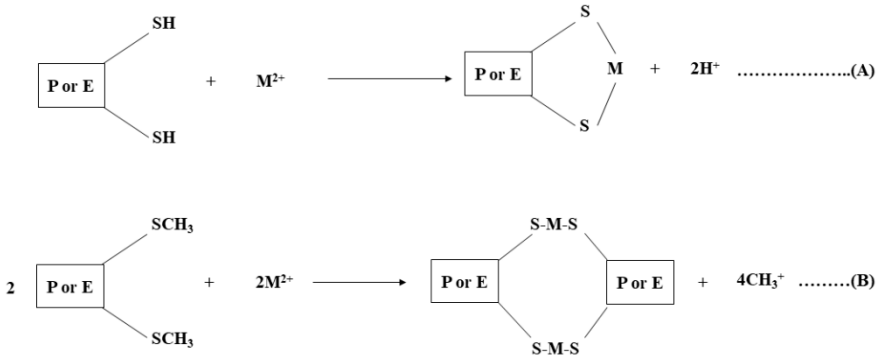

Scheme 1. Reactions representing the formation of bonds with the sulfhydryl groups (-SH) of cysteine and sulfur atoms of methionine (-SCH_3) (Duruibe et al., 2007) [14], where (**A**,**B**) are intramolecular bonding, P is protein, E is the enzyme, and M is metal. "Reprinted/adapted with permission from Ref. [14]. 2022, ACADEMIC JOURNALS".

Heavy metals can combine with antioxidants of the body and deactivate their activity. For example: In the reaction between heavy metal (M) and glutathione, the metal substitutes H atoms from SH groups on two adjacent glutathione molecules. The involvement of the two glutathione molecules in forming a strong bond with the metal renders them inactive for future reactions (Scheme 2) (Kamraj et al., 2012) [15].

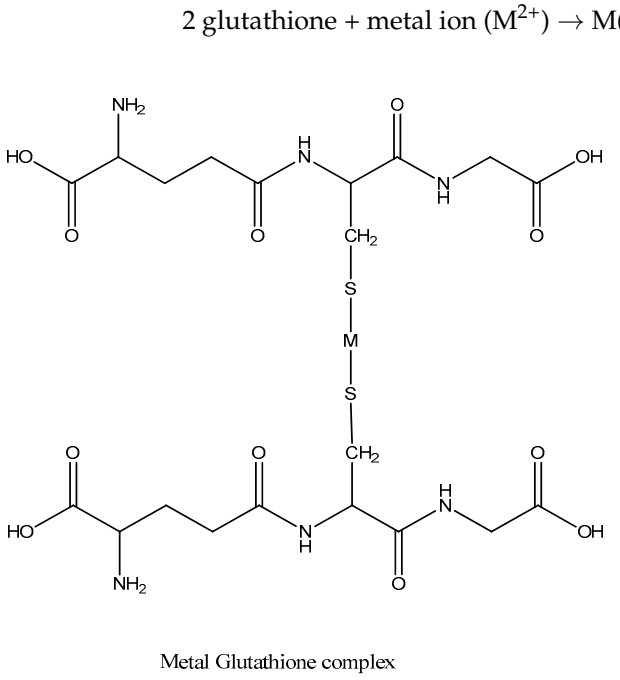

Scheme 2. Chemical structure of metal glutathione complex (Hajrat et al., 2019) [15]. "Reprinted/adapted with permission from Ref. [15]. 2022, Hindawi".

Mercury is caustic and carcinogenic with high cellular toxicity that can damage the kidney, nervous system, heart, and endocrine system [16]. Similarly, lead (Pb) is the second most abundant toxic element in the environment due to its use in gasoline, batteries, and pigments [17]. Lead can cause developmental, neurological, cardiovascular, and reproductive disorders even at low exposure levels [18]. Arsenic is a well-documented carcinogen, with over 200 million people worldwide exposed to arsenic-contaminated groundwater at concentrations above the WHO's permissible limit of 10 mg L^{-1} (10 ppb) [19].

The metal-based nanoparticles, including Au, Ag, Cu, Pt, and Pd, have gained attention because of their promising catalytic properties [20]. The metal nanoparticles-mediated reduction of 4-NP (nitrophenol) to 4-AP (aminophenol) was demonstrated for the first time in the presence of $NaBH_4$ [21]. The 4-NP to 4-AP alteration is thermodynamically achieved in the presence of $NaBH_4$ but kinetically restricted due to a lack of effective catalyst [22]. Green synthesized nanoparticles from various plant extracts have been examined for catalytic activity against various organic contaminant dyes in recent years.

Herein, we report the green synthesis and colorimetric metal sensing of biofunctionalized AgNPs from *Artemisia vulgaris* plant extracts. Green synthesized AgNPs colorimetric sensing potential was studied for Fe^{2+}, Ba^{2+}, Hg^{2+}, Cu^{2+}, Mn^{2+}, Zn^{2+}, As^{3+}, Ni^{2+}, Cr^{3+}, and Cd^{2+} metal ions. Similarly, AgNPs displayed catalytic reducing properties in converting 4-nitrophenol to 4-aminophenol.

2. Results and Discussion

2.1. Study of Optical Properties of AgNPs by UV-Vis Spectrometry

The formation of AgNPs was observed at room temperature by the change in color of the solution from yellow to reddish-brown by adding plant extract to 1 mM silver nitrate solution. The color formation might be due to the surface plasmon resonance (SPR) effect, and aqueous extracts change Ag^+ ions to Ag^0 [23]. The initial yellow color of the solution was observed as the plant extract was added drop by drop on a magnetic stirrer.

The reaction mixture (pH 10) was stirred for further 30 min; the solution turned to a brown color, as illustrated in Figure S1. Finally, the solution was incubated in the dark for 24 h at room temperature to reduce Ag^+ to Ag^0. The color of the mixture remained

unchanged, and no SPR band was observed at normal conditions (pH 6.4) even after 24 h. Hence, the pH of the solution mixture was maintained by adding 0.1 M NaOH. A sharp and narrow absorption peak was observed only at pH 10, which was not obtained at other pH values, as shown in Figure 1a.

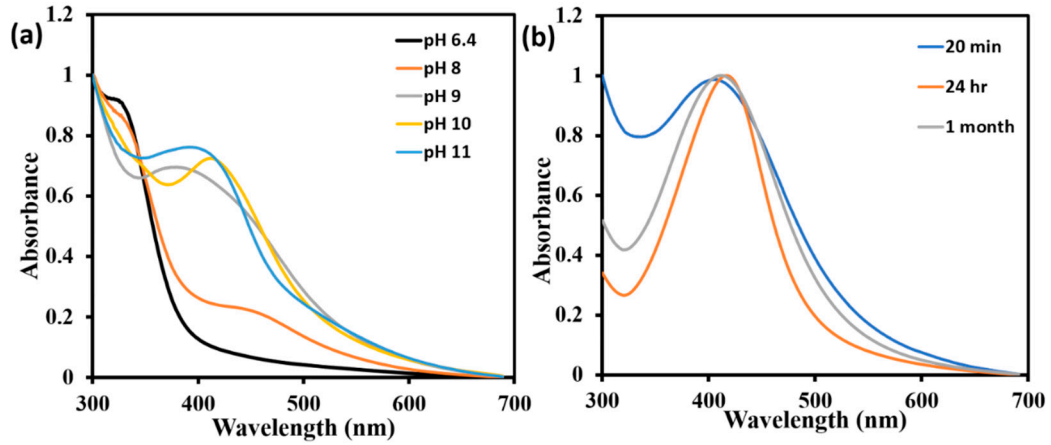

Figure 1. (**a**) UV–vis spectra of *Artemisia vulgaris*-mediated AgNPs at different pH and (**b**) UV–vis absorbed spectrum of *Artemisia vulgaris*-mediated AgNPs at different times.

The UV–vis spectra at different times is shown in Figure 1b. The characteristic UV absorption peak at 418 nm indicated the formation of AgNPs. The increase in the intensity of the spectrum with time could be due to the number of AgNPs forming due to the reduction of silver ions present in the aqueous solution. The UV-vis spectra of synthesized nanoparticles showed a single SPR band, indicating spherical-shaped nanoparticles present in the solution [24]. Even a month after their synthesis, the AgNPs were found stable in the solution of pH 10. By stability, we mean that there was no discernible change in the optical properties of the nanoparticle solutions over time.

2.2. Structural and Morphological Analysis

Scanning electron microscopy (SEM) analysis provides further insight into the morphology and size details of the silver nanoparticles. SEM images (Figure 2a,b) confirmed the formation of highly crystalline nanostructures, roughly spherical with various size distributions. The SEM image indicates the polycrystalline particles. The observation of larger nanoparticles may be attributed to AgNP's proclivity to agglomerate due to their high surface energy and ultra-fine nanoparticle high surface tension. The elemental composition of the green fabricated silver nanoparticles sample is shown by the energy dispersive X-ray (EDX) analysis spectrum (Figure 2c). Due to the SPR effect, the optical absorption peak at 3 keV and peaks at between 2 keV and 4 keV, associated with silver properties lines L and K, were found [25–27]. Such absorption peaks displayed the presence of silver in the nanostructure. In addition, other elements such as carbon (C) at 0.31 keV and oxygen (O) at 0.525 keV were also seen. In the tested samples, oxygen peaks appeared from the biomolecules bound to the silver nanoparticle surface. Therefore, the peak corresponding to C may be attributed to the conductive carbon tape.

Crystalline size and structure of the biosynthesized AgNPs were analyzed via XRD. AgNPs synthesized using *Artemisia vulgaris* extract were further demonstrated and confirmed by the characteristic peak observed in the XRD image (Figure 3a).

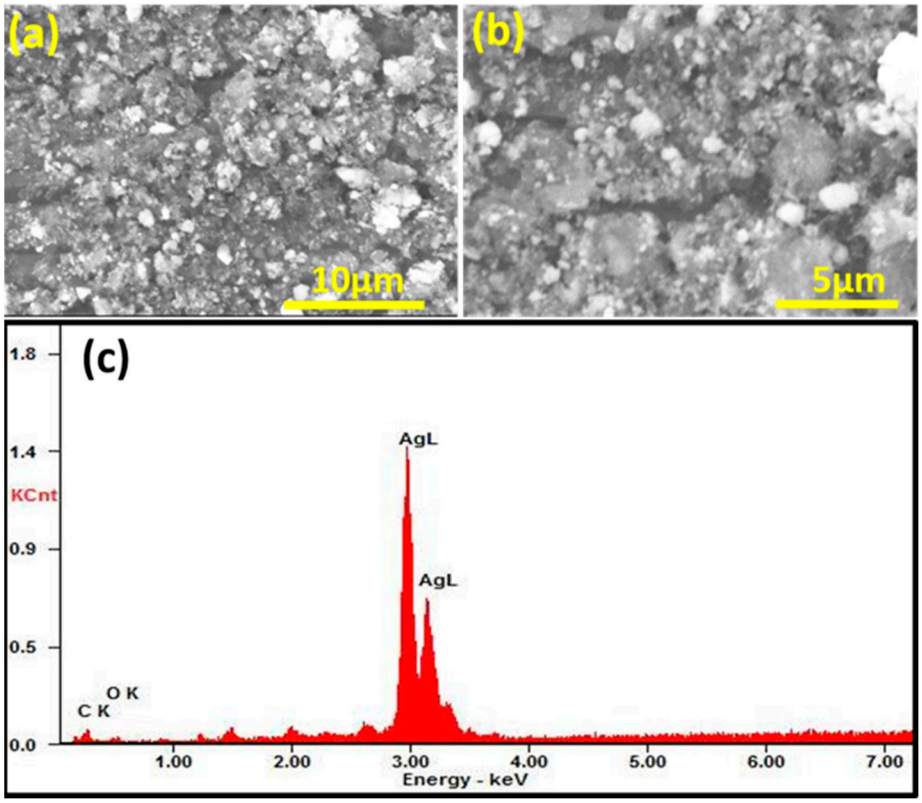

Figure 2. (**a**,**b**) SEM images of *Artemisia vulgaris*-mediated AgNPs at different magnification and (**c**) EDX spectrum of *Artemisia vulgaris*-mediated AgNPs.

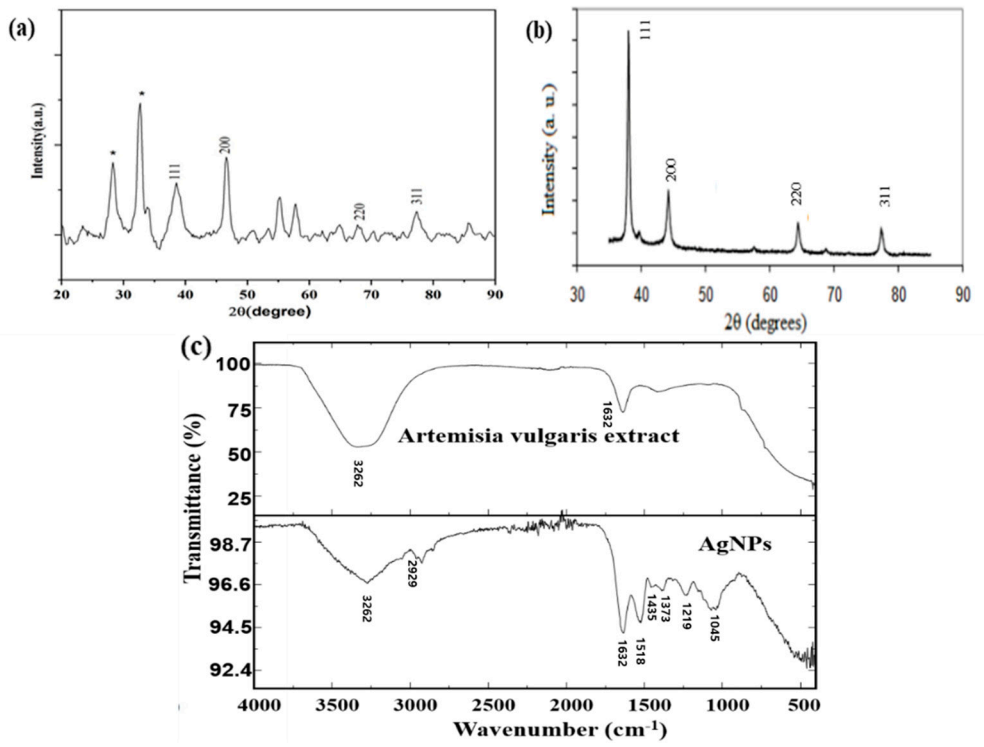

Figure 3. (**a**) XRD pattern of *Artemisia vulgaris*-mediated AgNPs, (**b**) XRD pattern of AgNPs [28], and (**c**) FTIR spectra of *Artemisia vulgaris* extract and AgNPs.

The four distinct diffraction peaks of the 2θ values of 38.260, 46.610, 67.440, and 77.700 can be indexed as (111), (200), (220), and (311), respectively. All diffraction peaks correspond to the characteristic face center cubic (FCC) silver lines, which is in good agreement with powder data of JCPDS file no. 84-0713. The XRD pattern shows that the AgNPs synthesized using *Artemisia vulgaris* are crystalline. The XRD is comparable to the reference presented in Figure 3b [28]. The asterisk (*) in Figure 3a are related to the impurities. The average crystallite size of Ag NPs was calculated from the FWHM of peaks using the Debye–Scherrer formula and was found to be 7 nm. SEM analysis is a more appropriate method for visualizing particle size, whereas XRD estimates the exact size of the NPs. In SEM images, it is seen that the agglomerate of the nanoparticles is formed. Thus, particle size differs from the Debye–Scherrer formula and SEM analysis. A few unassigned peaks (marked with stars) were also observed, indicating that bio-organic phase crystallization occurs on the surface of the silver nanoparticles and possibly silver oxide due to partial oxidation of silver. Similar spectra of silver nanoparticles synthesized using *Coleus aromaticus* leaf extract were reported [29].

FTIR spectra of both *Artemisia vulgaris* extract and biogenic AgNPs were analyzed to obtain information on the biomolecules' active functional groups in the bioreduction of Ag^+ and the capping of AgNPs. The FTIR analysis was performed in the range of 400 to 4000 cm^{-1}.

The FTIR spectra showed the absorption bands at 3262, 2929, 1632, 1518, 1435, 1373, 1219, and 1045 cm^{-1}, indicating the presence of capping agents with the nanoparticles (Figure 3c). In the case of AgNPs, the broad and strong band at 3262 cm^{-1} was assigned to O-H stretching vibration of alcohol and phenol. The bands at 2929 cm^{-1} and 2848 cm^{-1} correspond to the C-H stretching vibration of aromatic compounds [30]. The peaks observed at 1632 cm^{-1} were due to the presence of C-C and C-N stretching vibrations, indicating the presence of proteins, which was observed both in AgNPs and *Artemisia vulgaris* extract. [31]. The peak at 1435 cm^{-1} was assigned for N-H stretching vibrations present in the amide linkage of the proteins. The bands at 1373 cm^{-1} was designated for the proteins' N-H vibration. Moreover, the band at 1219 cm^{-1} was C-N stretching of amines. The broad, strong peak at 3262 cm^{-1} is weak in nanoparticles, which means the -OH group of the extract compounds is involved in reducing silver ions. The peak at 1045 cm^{-1} is attributed to the C-OH of the phenols, boosting the reduction of Ag^+ into Ag^0 through the sharing of polyphenols, such as flavonoids and triterpenoids. Such results come closer to the findings of Litvin and Minaev [32].

2.3. Analytical Application of Synthesized AgNPs

Synthesizing AgNPs using the plant extract is a cost-effective, eco-friendly, and fast technique used in this research. There could be many analytical applications of AgNPs in different sectors, some of which were studied in this work.

Colorimetric sensing of AgNPs

The selective colorimetric-sensing ability of the *Artemisia vulgaris*-mediated AgNPs for a series of heavy metals was explored in an aqueous solution. In this study, 10 different metal ions were used for colorimetric detection. Figure S2 showed the color change of AgNPs after adding a different heavy metal solution of 0.01 M concentration. There was a bathochromic shift in the λmax value and a decrease in absorbance of the AgNPs after adding a 0.01 M metal solution except for Hg^{2+}, as shown in Figure 4a. Due to the size effect, the UV absorption peak of Ag NPs is not fixed. The blue shift and red shift also occurred because of the same reason. The addition of Hg^{2+} selectively converted the reddish-brown-colored AgNPs solution into a completely colorless solution, which our naked eye can clearly distinguish, while observable color change was not obtained for the remaining metal solution.

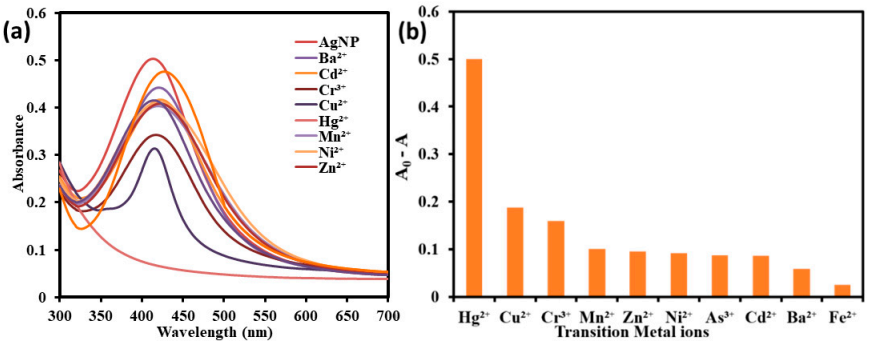

Figure 4. (**a**) UV-vis spectra of AgNPs dispersion with different metal ions and (**b**) absorption ratio of AgNPs with different metal ions.

There was no appreciable shift in the λmax value of AgNPs on the addition of Cu^{2+} (418 nm to 417 nm); however, the highest shifting was noticed for the Fe^{2+} (from 418 nm to 435 nm). A similar red shift in the SPR absorption of AgNPs from 418 nm to 430 nm was observed for Ni^{2+} and Zn^{2+} ions. When other metal ions Ba^{2+}, Cr^{3+}, Mn^{2+}, As^{3+}, and Cd^{2+} were added to AgNPs, shifting of λmax values from 418 nm to 426 nm, 423 nm, 428 nm, 421 nm, and 429 nm, respectively, were recorded.

There was no peak for the AgNPs dispersion with Hg^{2+} due to the interaction of the Hg^{2+} with the biomolecules adsorbed on the surface of AgNPs. Because of the strong SPR absorption band, the fresh biologically synthesized AgNPs were yellowish-brown in color. The yellow AgNPs solution became colorless in the presence of Hg^{2+}, accompanied by the broadening and blue shifting of the SPR band, indicating the selective sensitivity of AgNPs towards the Hg^{2+} ion.

The selective nature of green synthesized AgNPs with different metal ions was further studied by plotting AgNP solutions' absorbance with all-metal ions. The ΔA intensity ratio of AgNPs of different metal ions indicated the selectivity for Hg^{2+} ions, as illustrated in Figure 4b. The ΔA value of AgNPs with different metal ions was less than 0.2 except for Hg^{2+} ions, which was more than 0.5. This result showed that aggregated AgNPs (transparent color) accounted for a significant absorption ratio. In contrast, highly dispersed AgNPs had a lower ΔA value [33].

Sensitivity of AgNPs towards Hg^{2+} ions

The sensitive nature of the green synthesized AgNPs were examined by adding the different volumes of Hg^{2+} ions solutions to the 1 mL AgNPs dispersion at room temperature. The minimum detectable Hg^{2+} ion was identified within the aqueous system by a visible color change and monitored by the UV-vis spectra. There was a color change from yellowish-brown, yellow, light yellow, and light salmon to transparent after adding the different volumes of Hg^{2+} solutions incrementally from 20 to 600 µL, as illustrated in Figure S2a. Upon addition of 300 µL Hg^{2+}, the solution remained pale yellow; however, the solution turned colorless while adding 400 µL and a higher volume of Hg^{2+} solution in the first step of the experiment, as shown in Figure S2a.

In the second phase of the experiment, different volumes between 300 µL to 400 µL were added. When 380 µL Hg^{2+} (190 µM in terms of concentration) solution was added to AgNPs dispersion, the solution turned completely colorless, indicating the sensing range of the AgNPs as shown in Figure S2b.

After adding a different volume of Hg^{2+} ion solutions, the UV-vis spectra were recorded. It showed that the SPR band was blue-shifted with decreasing the intensity and broadening of the peak on increasing the volume of the Hg^{2+} ion solution, as illustrated in Figure 5a. The SPR band of AgNPs disappeared after adding the 250 µL and higher volume of Hg^{2+} solution (Figure 5a,b). It can be explained that the result obtained is possibly due to the redox reaction between the Hg^{2+} and Ag^{+}. Because of the higher reduction potential of Hg^{2+} ($E^0_{Hg2+/Hg}$ = +0.85 V) than Ag^0 ($E^0_{Ag+/Ag}$ = +0.80 V) [34], it

has a tendency to oxidize to Ag^{+}. The metallic mercury was formed after the reaction of AgNPs with Hg^{2+}. The newly formed metallic mercury could offer a strong bonding on the surface of silver and forms a layer around silver particle radiolytically, or an amalgam could be formed, which caused the blue shift and broadening of SPR band [35]. The plot of the λ_{max} against the volume of Hg^{2+} showed an exponential curve, as in Figure 5c. The maximum absorption value decreased with the volume of the Hg^{2+} ion.

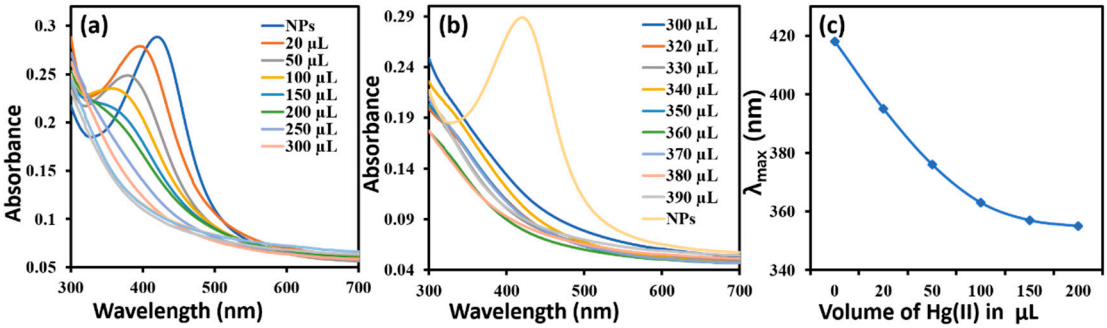

Figure 5. UV–vis spectra of AgNPs with (**a**) 20–200 µL of Hg^{2+}, (**b**) 300–400 µL of Hg^{2+}, and (**c**) variation of λmax on addition of Hg^{2+} solution.

Catalytic degradation of 4-nitrophenol (4-NP)

The catalytic activity of the AgNPs was examined by the reduction of 4-NP into 4-AP (aminophenol) in the presence of $NaBH_4$. The reduction was detected by observing the absorption on a UV-visible spectrophotometer. The absorption peak of 4-NP was shifted from 318 nm to 400 nm after the addition of $NaBH_4$ due to the formation of the 4-nitrophenolate ion. The absorption maximum at 400 nm was not decreased with time, as illustrated in Figure 6a. The $NaBH_4$ is inert to the aromatic compounds containing the $-NO_2$ groups, and this is because of the kinetic barrier between the BH_4^- and 4-NP [36]. The absorption intensity decreased rapidly within the 8 min by adding AgNPs, and a new peak was observed at 298 nm (Figure 6b). The new peak that appeared at 298 nm confirms the conversion of 4-NP to 4-AP [37].

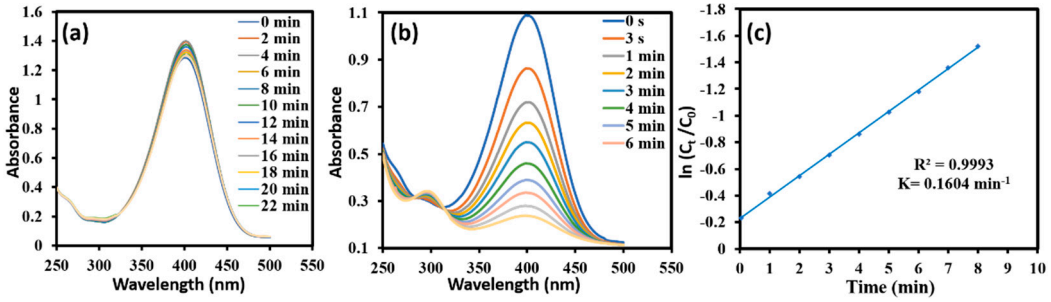

Figure 6. UV-vis spectrum of (**a**) 4-NP with $NaBH_4$ showing no reduction with time, (**b**) catalytic reduction of 4-NP with $NaBH_4$ by AgNPs, and (**c**) a plot of ln (C_t/C_0) against time on catalytic reduction of 4-NP.

The concentration of $NaBH_4$ was in a large excess of that of 4-NP. Thus, the reduction is a pseudo-first-order reaction concerning 4-NP alone. Therefore, the reaction kinetics can be described as:

$$\ln (C_t/C_0) = kt$$

where, k = apparent rate constant (min^{-1}), t = reaction time, and C_t and C_0 = concentrations of 4-NP at time t and 0, respectively.

The linear relationship between ln (C_t/C_0) and reaction time was observed, representing that the reduction of 4-NP follows the pseudo-first-order kinetics with a correlation

coefficient of 0.9993, as shown in Figure 6c. The rate constant k was calculated from the slope of the straight line and found to be 0.1604 min^{-1}.

3. Materials and Methods

The outline of the preparation of the plant extract and its commercial metal sensing application along with catalytic activity on the reduction of 4-Nitrophenol is presented in the Scheme 3.

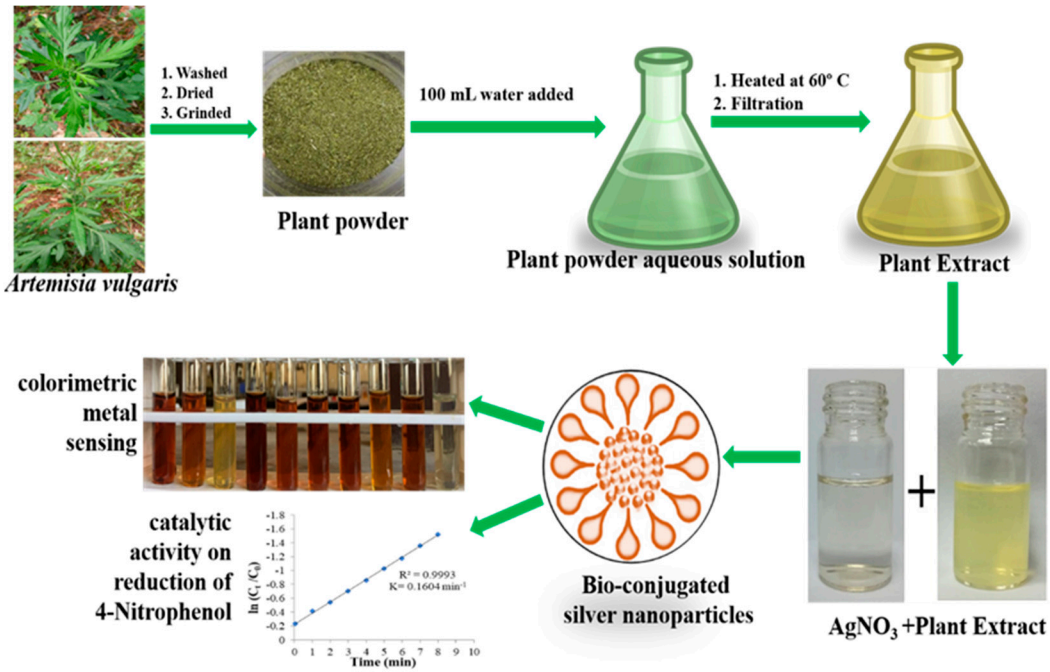

Scheme 3. Schematic diagram representing preparation of plant extract and its applications.

3.1. Plant Extract Preparation

Fresh leaves of *Artemisia vulgaris* were collected from the open spaces of the Kritipur, Kathmandu, with geographical distribution (27°40′54.62″N, 85°17′11.26″E). The clear digital images of the *Artemisia vulgaris* leaves are shown in Figure S3. The collected leaf was rinsed adequately with running tap water, followed by distilled water, and then dried at room temperature in the shade for two weeks. An electrical blender was used to grind the air-dried leaves into powder, then stored in polyethylene bags for future use. The leaf broth solution was prepared by adding 10 g of the final powder sample and 100 mL of distilled water. A magnetic stirrer stirred the solution at 60 °C for 45 min. After cooling, they were filtered through standard filter paper and Whatman Filter Paper No. 1. The filtrates were used for experiments, and the remaining extract was stored at 40 °C for further experiments.

3.2. Biosynthesis of Silver Nanoparticles

A stock solution of 50 mM $AgNO_3$ was prepared by dissolving 4.247 g of $AgNO_3$ in 500 mL distilled water in a volumetric flask. Next, 10 mL of stock solution was diluted to 500 mL to prepare 1 mM $AgNO_3$ to synthesize AgNPs. All the solutions in volumetric flasks were wrapped with a black covering and kept in the dark. Then, 10 mL of plant extract was added (drop-wise) to 90 mL aq. $AgNO_3$ solution was used for reducing Ag^+ on a magnetic stirrer for 25 min at room temperature and left in the dark for 24 h for further analysis. The pH of the solution was maintained at 10 by using the 0.1 M NaOH. The color change of the solution was observed. The UV–vis spectra were recorded at different time intervals to confirm the formation of AgNPs. The fully reduced solution after 24 h was centrifuged by Sorvall ST 8R centrifuge at 9000 rpm for 20 min at 25 °C. The supernatant

liquid was discarded, and the pellet obtained was redispersed in distilled water. The centrifugation process was repeated three times to wash off any adsorbed substance on the surface of silver nanoparticles and finally by absolute ethanol. Thus, purified AgNPs were dried at room temperature and stored in an Eppendorf tube covered with aluminum foil for further analysis.

3.3. Colorimetric Metal Sensing

After the different metal salt solutions were prepared, as explained in Section S2.6 of Supporting Information File, the colorimetric metal sensing was performed. In a regular sensing test, 1 mL of the metal solution was added to 4 mL of the noble metal nanoparticle dispersion. The ions used for the tests were Fe^{2+}, Ba^{2+}, Hg^{2+}, Cu^{2+}, Mn^{2+}, Zn^{2+}, As^{3+}, Ni^{2+}, Cr^{3+}, and Cd^{2+} at a concentration of 0.01 M. The color change of the resulting mixture was observed and analyzed by UV–vis spectrophotometry. Metal ions detected from the first stage of the experiment were further analyzed by lowering their concentration. To determine the detection limit of the synthesized AgNPs, different volumes (20–600 µL) of that metal ion were added to 1 mL of nanoparticle dispersion. The resulting dispersion was then analyzed by UV–vis spectrophotometry.

3.4. Catalytic Activity of the AgNPs

The catalytic role of the AgNPs was assessed using 4-NP by following the reported procedure with modifications [24] in the presence of $NaBH_4$. The experiment was performed by mixing 2.5 mL of freshly prepared 10 mM NaBH4, 200 µL of 1 mM 4-NP, and 10 µL of 1.5 mg mL^{-1} AgNPs suspension. Nanoparticle suspension was sonicated for 45 min before the experiment. The absorption of the mixture was monitored periodically at different time intervals between the ranges of 250 nm to 550 nm by using a UV–vis spectrophotometer. The stability of $NaBH_4$ with 4-NP was checked by scanning in the same range at different time intervals for 30 min before mixing the catalyst (AgNPs).

4. Conclusions

The current study concluded that the green synthesis of AgNPs, using *A. Vulgaris* extract as a reducing and capping agent, has advantages, such as ease of availability, eco-friendliness, and economic viability. Secondary metabolites were in charge of the green synthesis of AgNPs. More research is needed to determine the precise mechanism and to comprehend the entire process of green synthesis of silver NPs. The formation of AgNPs was confirmed by UV–vis spectroscopy in the aqueous medium. The synthesized AgNPs were further characterized by SEM, FTIR, and XRD, which also revealed the formation of AgNPs. The biosynthesized nanoparticle showed good sensing activity towards Hg^{2+}. The synthesized AgNPs exhibited a catalytic-reducing property in converting 4-NP to AP within 8 min. Therefore, green synthesized AgNPs could be employed to detect the hazardous Hg^{2+} ion in an aqueous medium to save the environment from mercury pollution and catalytic reduction of the organic dyes.

The present research work leaves the following prospects:

- Further optimization of protocol (effect of temperature, $AgNO_3$ concentration, plant extract concentration) is necessary for the large-scale production of the AgNPs.
- A comprehensive study is required to prepare the AgNPs-based sensor and application in catalysis.
- The toxicity should be tested for commercialization of the AgNPs.
- Besides the study of sensing and catalytic activity of AgNPs, other properties and their possible application should be studied.

Supplementary Materials: The following supporting information can be downloaded at: https://www.mdpi.com/article/10.3390/inorganics10080113/s1, Chemicals and reagents, various characterization techniques for silver nanoparticles (UV–vis Spectroscopy, Fourier-Transform Infra-Red (FTIR), X-ray Diffraction (XRD), Scanning Electron Microscope (SEM), Metal sensing activity of

AgNPs, preparation of metal salt solution, colorimetric metal sensing, and catalytic activity of the AgNPs) Figure S1: Color change during the synthesis of AgNPs nanoparticles; Figure S2: Color change on adding (a) 20–200 µL of Hg^{2+} and (b) 300–400 µL of Hg^{2+}; Figure S3: Photographic image of *Artemisia vulgaris*.

Author Contributions: Conceptualization, A.A. (Achyut Adhikari) and K.C.; data curation, A.A. (Achyut Adhikari), L.L., A.A.(Anup Adhikari), G.G., D.A., and E.R.B.; formal analysis, L.L. and A.A. (Anup Adhikari); funding acquisition, A.A. (Achyut Adhikari); investigation, A.A. (Achyut Adhikari), L.L., A.A. (Anup Adhikari), G.G., D.A., and E.R.B.; project administration, A.A. (Achyut Adhikari); resources, A.A. (Achyut Adhikari); supervision, K.C. and A.A. (Achyut Adhikari); validation, K.C. and A.A. (Achyut Adhikari); visualization, A.A. (Achyut Adhikari), L.L., and A.A. (Anup Adhikari); writing-riginal draft, A.A. (Achyut Adhikari), D.A., A.A. (Anup Adhikari), and L.L.; writing-review and editing, A.A. (Achyut Adhikari), K.C., and A.A. (Anup Adhikari). All authors have read and agreed to the published version of the manuscript.

Funding: We thank University Grant Commission (UGC), Nepal, for this work's partial funding (Award no.: MRS-75/76-S&T-14).

Institutional Review Board Statement: Not applicable.

Informed Consent Statement: Not applicable.

Data Availability Statement: Not applicable.

Acknowledgments: We would like to thank the National Academy of Science and Technology (NAST), Lalitpur, Nepal, for the XRD analysis.

Conflicts of Interest: The authors declare no conflict of interest.

References

1. Kharissova, O.V.; Dias, H.V.R.; Kharisov, B.I.; Pérez, B.O.; Pérez, V.M.J. The greener synthesis of nanoparticles. *Trends Biotechnol.* **2013**, *31*, 240–248. [CrossRef]
2. Zhang, X.-F.; Liu, Z.-G.; Shen, W.; Gurunathan, S. Silver Nanoparticles: Synthesis, Characterization, Properties, Applications, and Therapeutic Approaches. *Int. J. Mol. Sci.* **2016**, *17*, 1534. [CrossRef]
3. Rauwel, P. Emerging Trends in Nanoparticle Synthesis Using Plant Extracts for Biomedical Applications. *Glob. J. Nanomed.* **2017**, *1*, 5555562.
4. Phuyal, S.; Lamichhane, G.; Gupta, A.; Khadayat, K.; Adhikari, A.; Marahatha, R.; Khadka, S.; Parajuli, N. Biosynthesis of Silver Nanoparticles from Rhododendron arboreum for Metal Sensing, Antibacterial Assessment, and Photocatalytic Degradation. *J. Nanomater.* **2022**, *2022*, 2110636. [CrossRef]
5. Chapagain, A.; Acharya, D.; Das, A.K.; Chhetri, K.; Oli, H.B.; Yadav, A.P. Alkaloid of Rhynchostylis retusa as Green Inhibitor for Mild Steel Corrosion in 1 M H_2SO_4 Solution. *Electrochem* **2022**, *3*, 211–224. [CrossRef]
6. Rajeshkumar, S.; Bharath, L.V. Mechanism of plant-mediated synthesis of silver nanoparticles-A review on biomolecules involved, characterisation and antibacterial activity. *Chem. Biol. Interact.* **2017**, *273*, 219–227. [CrossRef] [PubMed]
7. Singh, P.; Kim, Y.J.; Zhang, D.; Yang, D.C. Biological Synthesis of Nanoparticles from Plants and Microorganisms. *Trends Biotechnol.* **2016**, *34*, 588–599. [CrossRef] [PubMed]
8. Nadzir, M.M.; Idris, F.N.; Hat, K. Green synthesis of silver nanoparticle using Gynura procumbens aqueous extracts. *AIP Conf. Proc.* **2019**, *2124*, 030018.
9. Patil, S.V.; Borase, H.P.; Patil, C.D.; Salunke, B.K. Biosynthesis of silver nanoparticles using latex from few euphorbian plants and their antimicrobial potential. *Appl. Biochem. Biotechnol.* **2012**, *167*, 776–790. [CrossRef]
10. Logaranjan, K.; Devi, S.; Pandian, K. Biogenic Synthesis of Silver Nanoparticles Using Fruit Extract of Ficus Carica and Study Its Antimicrobial Activity. *Nano Biomed. Eng.* **2012**, *4*, 177–182. [CrossRef]
11. Aravinthan, A.; Govarthanan, M.; Selvam, K.; Praburaman, L.; Selvankumar, T.; Balamurugan, R.; Kamala-Kannan, S.; Kim, J.-H. Sunroot mediated synthesis and characterization of silver nanoparticles and evaluation of its antibacterial and rat splenocyte cytotoxic effects. *Int. J. Nanomed.* **2015**, *10*, 1977.
12. Sable, N.; Gaikwad, S.; Bonde, S.; Gade, A.; Rai, M. Phytofabrication of silver nanoparticles by using aquatic plant Hydrilla verticillata. *Nusant. Biosci.* **2012**, *4*, 45–49. [CrossRef]
13. Bar, H.; Bhui, D.K.; Sahoo, G.P.; Sarkar, P.; De, S.P.; Misra, A. Green synthesis of AgNPs using latex of Jatropha curcas. *Colliod Surf. A* **2009**, *39*, 134–139. [CrossRef]
14. Duruibe, J.O.; Ogwuegbu, M.O.C.; Egwurugwu, J.N. Heavy metal pollution and human biotoxic effects. *Int. J. Phys. Sci.* **2007**, *2*, 112–118.
15. Hajraj, A.; Ezzat, K.; Ikram, I. Environmental Chemistry and Ecotoxicology of Hazardous Heavy Metals: Environmental Persistence, Toxicity, and Bioaccumulation. *J. Chem.* **2019**, *2019*, 6730305.

16. MubarakAli, D.; Thajuddin, N.; Jeganathan, K.; Gunasekaran, M. Plant extract mediated synthesis of silver and gold nanoparticles and its antibacterial activity against clinically isolated pathogens. *Colloids Surf. B Biointerfaces* **2011**, *85*, 360–365. [CrossRef] [PubMed]
17. Roni, M.; Murugan, K.; Panneerselvam, C.; Subramaniam, J.; Hwang, J.-S. Evaluation of leaf aqueous extract and synthesized silver nanoparticles using Nerium oleander against *Anopheles stephensi* (Diptera: *Culicidae*). *Parasitol. Res.* **2013**, *112*, 981–990. [CrossRef] [PubMed]
18. Ramteke, C.; Chakrabarti, T.; Sarangi, B.K.; Pandey, R.-A. Synthesis of Silver Nanoparticles from the Aqueous Extract of Leaves of Ocimum sanctum for Enhanced Antibacterial Activity. *J. Chem.* **2013**, *2013*, 278925. [CrossRef]
19. Jacob, S.J.P.; Finub, J.S.; Narayanan, A. Synthesis of silver nanoparticles using Piper longum leaf extracts and its cytotoxic activity against Hep-2 cell line. *Colloids Surf. B Biointerfaces* **2012**, *91*, 212–214. [CrossRef]
20. Karthiga, D.; Anthony, S.P. Selective colorimetric sensing of toxic metal cations by green synthesized silver nanoparticles over a wide pH range. *RSC Adv.* **2013**, *3*, 16765–16774. [CrossRef]
21. Nipane, S.V.; Mahajan, P.G.; Gokavi, G.S. Green synthesis of silver nanoparticle in calotropis procera flower extract and its application for Fe^{2+} sensing in aqueous solution. *Int. J. Recent Innov. Trends Comput. Commun* **2016**, *4*, 98–107.
22. Hoyos, L.E.S.; Sánchez-Mendieta, V.; Vilchis-Nestor, A.R.; Camacho-López, M.A. Biogenic silver nanoparticles as sensors of Cu^{2+} and Pb^{2+} in aqueous solutions. *Univers. J. Mater. Sci.* **2017**, *5*, 29–37.
23. Wu, T.; Liu, C.; Tan, K.J.; Hu, P.P.; Huang, C.Z. Highly selective light scattering imaging of chromium (III) in living cells with silver nanoparticles. *Anal. Bioanal. Chem.* **2010**, *397*, 1273–1279. [CrossRef] [PubMed]
24. Kumar, B.; Smita, K.; Cumbal, L.; Debut, A. Synthesis of silver nanoparticles using Sacha inchi (*Plukenetia volubilis* L.) leaf extracts. *Saudi J. Biol. Sci.* **2014**, *21*, 605–609. [CrossRef] [PubMed]
25. Dubey, S.P.; Lahtinen, M.; Sillanpää, M. Green synthesis and characterizations of silver and gold nanoparticles using leaf extract of Rosa rugosa. *Colloids Surf. A Physicochem. Eng. Asp.* **2010**, *364*, 34–41. [CrossRef]
26. Raman, C.; Goldsmith, M.R.; Agunbiade, T.A. *Short Views on Insect Genomics and Proteomics*; Springer: Berlin/Heidelberg, Germany, 2015; pp. 112–115.
27. Govindarajan, M.; Rajeswary, M.; Veerakumar, K.; Muthukumaran, U.; Hoti, S.L.; Benelli, G. Green synthesis and characterization of silver nanoparticles fabricated using Anisomeles indica: Mosquitocidal potential against malaria, dengue and Japanese encephalitis vectors. *Exp. Parasitol.* **2016**, *161*, 40–47. [CrossRef] [PubMed]
28. Alzoubi, F.Y.; Bidier, S.A.A. Characterization and Aggregation of Silver Nanoparticles Dispersed in an Aqueous Solution. *Chin. J. Phys.* **2013**, *51*, 378–387.
29. Vanaja, M.; Annadurai, G. Coleus aromaticus leaf extract mediated synthesis of silver nanoparticles and its bactericidal activity. *Appl. Nanosci.* **2013**, *3*, 217–223. [CrossRef]
30. Gautam, K.P.; Acharya, D.; Bhatta, I.; Subedi, V.; Das, M.; Neupane, S.; Kunwar, J.; Chhetri, K.; Yadav, A.P. Nickel Oxide-Incorporated Polyaniline Nanocomposites as an Efficient Electrode Material for Supercapacitor Application. *Inorganics* **2022**, *10*, 86. [CrossRef]
31. Prakash, P.; Gnanaprakasam, P.; Emmanuel, R.; Arokiyaraj, S.; Saravanan, M. Green synthesis of silver nanoparticles from leaf extract of Mimusops elengi, Linn. for enhanced antibacterial activity against multi drug resistant clinical isolates. *Colloids Surf. B Biointerfaces* **2013**, *108*, 255–259. [CrossRef] [PubMed]
32. Litvin, V.A.; Minaev, B.F. Spectroscopy study of silver nanoparticles fabrication using synthetic humic substances and their antimicrobial activity. *Spectrochim. Acta Part A Mol. Biomol. Spectrosc.* **2013**, *108*, 115–122. [CrossRef] [PubMed]
33. Guo, Y.; Wang, Z.; Qu, W.; Shao, H.; Jiang, X. Colorimetric detection of mercury, lead and copper ions simultaneously using protein-functionalized gold nanoparticles. *Biosens. Bioelectron.* **2011**, *26*, 4064–4069. [CrossRef] [PubMed]
34. Alshawi, J.M.S.; Mohammed, M.Q.; Alesary, H.F.; Ismail, H.K.; Barton, S. Voltammetric Determination of Hg^{2+}, Zn^{2+}, and Pb^{2+} Ions Using a PEDOT/NTA-Modified Electrode. *ACS Omega* **2022**, *7*, 20405–20419. [CrossRef] [PubMed]
35. Katsikas, L.; Gutiérrez, M.; Henglein, A. Bimetallic colloids: Silver and mercury. *J. Phys. Chem.* **1996**, *100*, 11203–11206. [CrossRef]
36. Dotzauer, D.M.; Dai, J.; Sun, L.; Bruening, M.L. Catalytic membranes prepared using layer-by-layer adsorption of polyelectrolyte/metal nanoparticle films in porous supports. *Nano Lett.* **2006**, *6*, 2268–2272. [CrossRef]
37. Qian, H.; He, Q.; Zheng, J.; Li, S.; Zhang, S. Catechol-functionalized microporous organic polymer as supported media for Pd nanoparticles and its high catalytic activity. *Polymer* **2014**, *55*, 550–555. [CrossRef]